PNAS RESEARCH ARTICLE | CHEMISTRY

Examining atherosclerotic lesions in three dimensions at the nanometer scale with cryo-FIB-SEM

Jenny Capua-Shenkar[a], Neta Varsano[a], Noya-Ruth Itzhak[a], Ifat Kaplan-Ashiri[b], Katya Rechav[b], Xueting Jin[c], Manabu Niimi[d], Jianglin Fan[d], Howard S. Kruth[c], and Lia Addadi[a,1]

Contributed by Lia Addadi; received March 29, 2022; accepted July 7, 2022; reviewed by George Abela and Joanna Aizenberg

We employed in a correlative manner an unconventional combination of methods, comprising cathodoluminescence, cryo–scanning electron microscopy (SEM), and cryo–focused ion beam (FIB)-SEM, to examine the volumes of thousands of cubed micrometers from rabbit atherosclerotic tissues, maintained in close-to-native conditions, with a resolution of tens of nanometers. Data from three different intralesional regions, at the media–lesion interface, in the core, and toward the lumen, were analyzed following segmentation and volume or surface representation. The media–lesion interface region is rich in cells and lipid droplets, whereas the core region is markedly richer in crystals and has lower cell density. In the three regions, thin crystals appear to be associated with intracellular or extracellular lipid droplets and multilamellar bodies. Large crystals are independently positioned in the tissue, not associated with specific cellular components. This extensive evidence strongly supports the idea that the lipid droplet surfaces and the outer membranes of multilamellar bodies play a role in cholesterol crystal nucleation and growth and that crystal formation occurs, in part, inside cells. The correlative combination of methods that allowed the direct examination of cholesterol crystals and lipid deposits in the atherosclerotic lesions may be similarly used for high-resolution examination of other tissues containing pathological or physiological cholesterol deposits.

cholesterol crystals | atherosclerosis in rabbit models | cathodoluminescence | correlative electron microscopy | lipid droplet

Significance

Cholesterol crystallization is crucial in the development of atherosclerosis. Cholesterol crystals contribute to the rupture of the atherosclerotic plaque, which can result in myocardial infarction and stroke. Cholesterol crystallization is associated with intralesional macrophages; however, where and how crystallization occurs is still unclear. We developed a combination of advanced techniques of scanning electron microscopy to produce nanometer-resolution two-dimensional and three-dimensional images of atherosclerotic lesions in rabbits, with tissue and crystals preserved in close-to-native conditions. We bring evidence that cholesterol crystals nucleate on lipid droplets and that crystal formation can occur intracellularly. These observations, made possible by observing cryo-fixed unembedded and unprocessed tissues, advance our understanding of crystal formation processes in atherosclerosis.

Cholesterol crystallization plays a significant role in the pathogenesis and the clinical manifestation of atherosclerosis (1, 2). Cholesterol crystals exert physical damage to the soft matrix environment, because of their shape and rigidity; they also cause and enhance inflammation (1, 3–5). Cholesterol crystals, once formed, are very difficult to dissolve and are thus coresponsible for the deleterious effects of embolism following plaque rupture (6–9). Crystalline cholesterol is mostly associated with advanced atherosclerotic lesions; however, studies performed in murine models suggest that crystal deposition can occur also in early stages of lesion formation (4, 5). Atherosclerotic lesions form in the subendothelial layer of the blood vessel walls, within the tunica intima, and adjacent to the tunica media (Fig. 1 *A* and *C*).

During the initial stages of atherosclerosis, imbalance between the uptake of low-density lipoproteins (LDL) and cholesterol efflux leads to the deposition of esterified cholesterol in the form of lipid droplets inside macrophages, transforming them into the so-called foam cells (10, 11). After engulfment, LDL are transferred to late endosomes/lysosomes where lysosomal acid lipase hydrolyzes cholesteryl esters to generate free (unesterified) cholesterol. Free cholesterol is then shuttled to the endoplasmic reticulum, reesterified by Acetyl-CoA Acetyltransferase 1, and stored in lipid droplets (11). In the lipid droplets, neutral cholesteryl ester hydrolase hydrolyzes excess cholesteryl esters, generating, yet again, free cholesterol, which moves to the plasma membrane, where it is taken up by cholesterol acceptors (10–12). The balance between hydrolysis and esterification of cholesterol plays a key role in maintaining cellular cholesterol homoeostasis, as free cholesterol overload may lead to the formation of cholesterol crystals (11, 13). Cholesterol ester crystals were never detected in atherosclerotic lesions (14).

Cholesterol crystals were observed in the inner compartment of multilamellar bodies in atherosclerotic lesions of rabbits (15). In macrophage model systems, crystalline cholesterol appeared in locations associated with secondary lysosomal compartments and cellular membranes (16–19). In cultured hepatocytes as well as in hepatic tissues, cholesterol crystals were reported to be associated with lipid droplets (20, 21). Recently, Lehti et al. reported cholesterol crystal association with lipid droplets in the extracellular compartment of a human atherosclerotic lesion (22). In human lesions, cholesterol crystals appear associated with foam cells both in intra- and in extracellular locations (11, 23). The lesions grow over decades, with concurrent gradual modifications, and

Author contributions: J.C.-S., H.S.K., and L.A. designed research; J.C.-S. performed research; I.K.-A., K.R., X.J., M.N., and J.F. contributed new reagents/analytic tools; J.C.-S., N.V., N.-R.I., and L.A. analyzed data; and J.C.-S., N.V., and L.A. wrote the paper.

Reviewers: G.A., Michigan State University; and J.A., Harvard University.

The authors declare no competing interest.

[1]To whom correspondence may be addressed. Email: Lia.Addadi@weizmann.ac.il.

This article contains supporting information online at http://www.pnas.org/lookup/suppl/doi:10.1073/pnas.2205475119/-/DCSupplemental.

Published August 8, 2022.

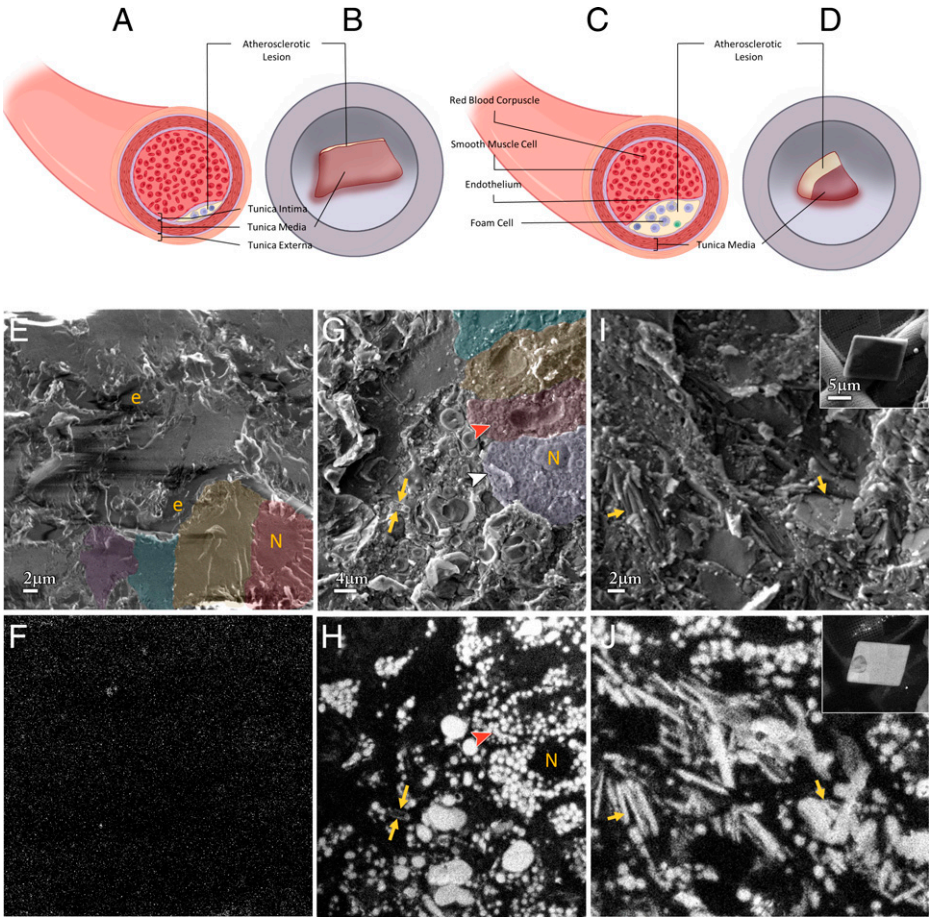

Fig. 1. Cryo-SEM and CL of freeze-fractured tissues of atherosclerotic lesions. (*A*–*D*) Schematic representations of lesion locations in the tissue. *B* and *D* are schematic representations of the samples of tissue slices examined in cryo-SEM-CL below. *B* refers to *G* and *H* and *D* to *I* and *J* and *SI Appendix*, Fig. S3. (*A* and *B*) Less-severe lesion. (*C* and *D*) More-severe lesion. (*E* and *F*) Cryo-SEM (*E*) and cryo-CL (*F*) images of the same region from the aorta of a control rabbit. Four cells are highlighted with different pseudocolors. e, elastic fibers; N, cell nucleus. (*G* and *H*) Cryo-SEM (*G*) and cryo-CL (*H*) images from the same region of a thin atherosclerotic lesion as in *A* and *B*, taken from the descending aorta ([*b*] in *SI Appendix*, Fig. S1*A*) of an affected rabbit. Four foam cells are highlighted with different pseudocolors. Arrowheads: white, plasma membrane; red, lipid droplet; yellow arrows, cholesterol crystals; N, cell nucleus. (*I* and *J*) cryo-SEM (*I*) and cryo-CL (*J*) images from the same region of a thick lesion as in *C* and *D*, taken from the ascending aorta of an affected rabbit ([*a*] in *SI Appendix*, Fig. S1*A*). Yellow arrows, cholesterol crystals. (*Insets*) SEM and CL of a synthetic crystal of cholesterol. *A*–*D* were created with BioRender.com.

this makes reconstruction of the mechanism(s) of cholesterol crystal deposition extremely difficult. Rabbit animal models present one of the best-known models for accelerated atherosclerosis, due to a lipid metabolism and lipoprotein profile very similar to those in humans (24, 25). In rabbits, there is a spontaneous development of atherosclerotic lesions following the administration of a high-cholesterol diet, as occurs in human subjects over much longer periods of time (6, 24). Human and rabbit atheromas are characterized by very similar cholesterol crystal morphologies, as well as by the presence of liquid crystals of cholesteryl esters (26). Rabbit models therefore provide the opportunity to ask specific questions concerning cholesterol crystallization in atherosclerosis over relatively short periods.

Conventional electron microscopy techniques provide fine structural detail of cells and cell organelles. However, due to the required sample processing, especially dehydration and use of organic solvents, lipid materials dissolve, such that lipid droplets and cholesterol crystals appear as voids (9, 11, 23, 27). In fact, an elongated void in a 70-nm-thick transmission electron microscopy (TEM) section may represent a section through a cholesterol crystal, as well as a section through an elongated vesicle or lipid droplet or even a discontinuation in the tissue, whether innate or due to drying.

In order to overcome this challenge, we employed cryo-preservation techniques to maintain intact cholesterol-related structures, hydrated and close to their native state, with minimal processing not involving the use of organic solvents (28, 29). We developed a correlative workflow using cathodoluminescence (CL) in conjunction with cryo–scanning electron microscopy (cryo-SEM), which allowed the detection of cholesterol aggregates in the organic tissue at high spatial resolution. With the support of the correlative workflow, we achieved three-dimensional (3D) reconstructions of the lesion tissues using cryo–focused ion beam SEM (cryo-FIB-SEM), an innovative high-resolution imaging technique that allows 3D exploration of large tissue volumes at nanometer resolution (30–32). The complexity of the procedures does not allow statistical collection of data. Rather, we can derive mechanistic hypotheses from the observations, because large volumes of tissue are examined in close-to-original conditions, with all the components preserved. Our observations indicate an important role of intralesional lipid droplets and multilamellar bodies as potential sites for cholesterol nucleation in the course of atherosclerosis.

Results

Aortic tissues of 12-week-old male New Zealand White rabbits fed with cholesterol-enriched diet were examined and compared to the aortic tissues of rabbits fed with a normal chow (for additional details on all procedures see *Materials and Methods*).

Histological comparison of tissues taken from two different aortic regions (*SI Appendix*, Fig. S1*A*) of the two rabbit groups shows that rabbits fed with normal chow diet display a normal healthy intima, with no apparent lipid deposits in any of the regions of interest (*SI Appendix*, Fig. S1 *B* and *C*). Conversely, tissues from the aorta of rabbits fed with cholesterol diet have a thickened intima, foam cells, and lipid deposition in the subendothelial regions (*SI Appendix*, Fig. S1 *D* and *E* and Fig. 1 *A* and *C*). Thicker and more substantial lesions were observed in the ascending aortic region (*SI Appendix*, Fig. S1 *A*, [*a*]). These observations are in good agreement with previous studies (33, 34).

In the next step, chemically fixed tissues of rabbits fed with cholesterol-enriched diet and of control rabbits were high-pressure-frozen to produce vitrified samples, were freeze-fractured, and were observed using cryo-SEM and CL (*SI Appendix*, Fig. S2 and Fig. 1 *E–J*). Cryo-SEM allows observation of hydrated tissues, preserved in conditions close to their native state. CL allows identification of cholesterol and cholesteryl ester deposits that, owing to their material properties, emit luminescence upon excitation with an electron beam (Fig. 1 *F*, *H*, and *J*, *Inset* and *SI Appendix*, Fig. S2 *B*, *D*, and *F*) (35–38).

At low magnifications, the healthy aortic tissue exhibits distinct tissue borders and clearly distinguished layers in the blood vessel wall (*SI Appendix*, Fig. S2*A*; schematics of the unaffected region in Fig. 1 *A* and *C*). The intima and the adventitia are easily identified as the inner and outer vessel borders, respectively. The media layer occupies the largest portion of the vessel wall and has a characteristic striation produced by the presence of the elastic fibers (Fig. 1*E* and *SI Appendix*, Fig. S2*A*). The normal tissue has only a basal and negligible CL signal, with no detectable light-emitting cholesterol and cholesteryl ester deposits (Fig. 1*F* and *SI Appendix*, Fig. S2*B*).

The aortic tissues of the rabbit fed with cholesterol diet displayed apparent tissue architecture loss, so much so that the different layers of the blood vessel were difficult to detect (*SI Appendix*, Fig. S2 *C* and *E*; schematics in Fig. 1 *A* and *C*). The lesion boundaries could not be detected using cryo-SEM alone, but using CL the lesion and its boundaries were easily detected (*SI Appendix*, Fig. S2 *D* and *F*). The two lesions from two different aortic regions differed in the extent of the lesion and in lesion content. Sparse cholesterol deposits were also observed in the subintimal region, but most of the tunica media region was clear of cholesterol deposits (*SI Appendix*, Fig. S2*F*).

At higher magnification, the control tissue shows distinct cells with no CL signal altogether (Fig. 1 *E* and *F*). In contrast to the control tissue, in the least-affected regions of the lesions abundant foam cells appear (Fig. 1 *G* and *H*). The foam cells have a continuous plasma membrane, clearly defined nuclei, and are filled with lipid droplets with high CL signal (Fig. 1 *G* and *H*). Crystalline cholesterol with detectable CL is present in limited amounts, and the few detectable crystals are located in close proximity to lipid droplets (Fig. 1 *G* and *H*, yellow arrows). Most lipid droplets have round morphology, although a smaller population of lipid droplets has considerably larger sizes and distorted morphology. Conversely, the most affected regions of the lesion display higher level of loss of architecture. Cell membranes, if at all visible, are not continuous, and cholesterol crystals with high CL signal are abundant, mostly assembled in stacks (Fig. 1 *I* and *J*).

To understand the contextual interplay between crystalline cholesterol and the different cellular structures, we employed cryo-FIB-SEM block face serial imaging on an aortic tissue taken from the ascending thoracic aorta of a rabbit fed with cholesterol-rich diet (Fig. 2). The technique consists in alternating removal of 10-nm thin slices of material with an FIB, and imaging of the exposed slice with SEM, while all the procedure occurs at cryo-conditions on high-pressure-frozen tissue (30–32). The resulting stacks of >1,000 images are used to reconstruct in 3D relatively large volumes of tissue (tens of micrometers in 3D). The analyzed tissue was kept through the whole process in close-to-native conditions, without any prior chemical processing, drying, or use of dyes, apart from chemical fixation (*Materials and Methods*).

In order to choose the regions of interest for 3D examination, we developed a correlative approach involving the use of cryo-SEM combined with CL, prior to the cryo-FIB-SEM procedure. The lesion (schematic in Fig. 1 *C* and *D* and images in Fig. 1 *I* and *J*) was first examined in the cryo-SEM/CL electron microscope (*SI Appendix*, Fig. S3 *A–D*), and the regions where we wished to perform 3D imaging were identified. The specimens were then transferred to the FIB-SEM instrument, while maintaining cryogenic conditions. Trenches were carved and data collection was performed using the FIB-SEM milling and imaging procedure (*SI Appendix*, Fig. S3*E*). Because of the complexity of the correlative cryo-SEM, CL, and cryo-FIB-SEM procedure, only a limited number of regions can be imaged. Therefore, we adopted the strategy to examine three representative regions in one atherosclerotic lesion, which allowed comparing between the characteristics of the different locations. The three regions are L, the region adjacent to the lumen of the vessel, C, the core of the lesion, and M, the region at the interface of the lesion with the tunica media of the blood vessel (*SI Appendix*, Fig. S3*E*). Three stacks of images were collected, comprising in region L = 1,190 images, in region C = 1,129 images and in region M = 1,407 images, encompassing volumes of $25.38 \times 14.32 \times 11.9\ \mu m^3$, $41.02 \times 16.82 \times 11.29\ \mu m^3$, and $37.42 \times 12.13 \times 14.07\ \mu m^3$ in the three regions, respectively. The stacks of images were aligned and processed for removal of artifacts, after which the reconstructed planes were examined (*Materials and Methods*).

Atherosclerotic tissues present a big challenge in data analysis of cryo-FIB-SEM, due to pronounced artifacts derived from the pathology of the tissue, loaded with crystals and lipid deposits. The most frequent problems in cryo-FIB-SEM in general, which are magnified in these tissues, are curtaining, which produces vertical periodical lines caused by ion beam milling, and charging (*SI Appendix*, Fig. S4, yellow, white, and red arrowheads) (30–32). Despite the fact that we applied advanced procedures to eliminate the different artifacts, some data could not be fully repaired.

Two-dimensional cryo-FIB-SEM representative slices M, C, and L and volume segmentations M_{vol}, C_{vol}, and L_{vol} of the three regions of interest are shown in Fig. 2. In cryo-FIB-SEM, the image contrast derives from differences in surface potential; consequently, cholesterol crystals, lipid droplets, and membranes that are mainly hydrophobic appear dark because they absorb electrons, whereas polar, negatively charged regions are bright because they repel electrons (31). Some lipid droplets display a bright core, related to either content, density, or structural core/shell differences (39) (Fig. 2, M, red arrows).

The differences between the three regions are evident. The media–lesion interface region (Fig. 2, M and M_{vol}) is rich in cells with clearly detectable intact nuclei and is rich in lipid droplets, occupying 12% of the total volume. There are crystals, but not in large amounts (1% of the total volume). The C region has lower amount of lipid droplets than the M region (7% of the total volume), and few detectable cell nuclei (Fig. 2, C and C_{vol}). Packed cholesterol crystals dominate, occupying 16% of the total volume. The L region is intermediate between the previous two, with large crystals (8% of the total volume),

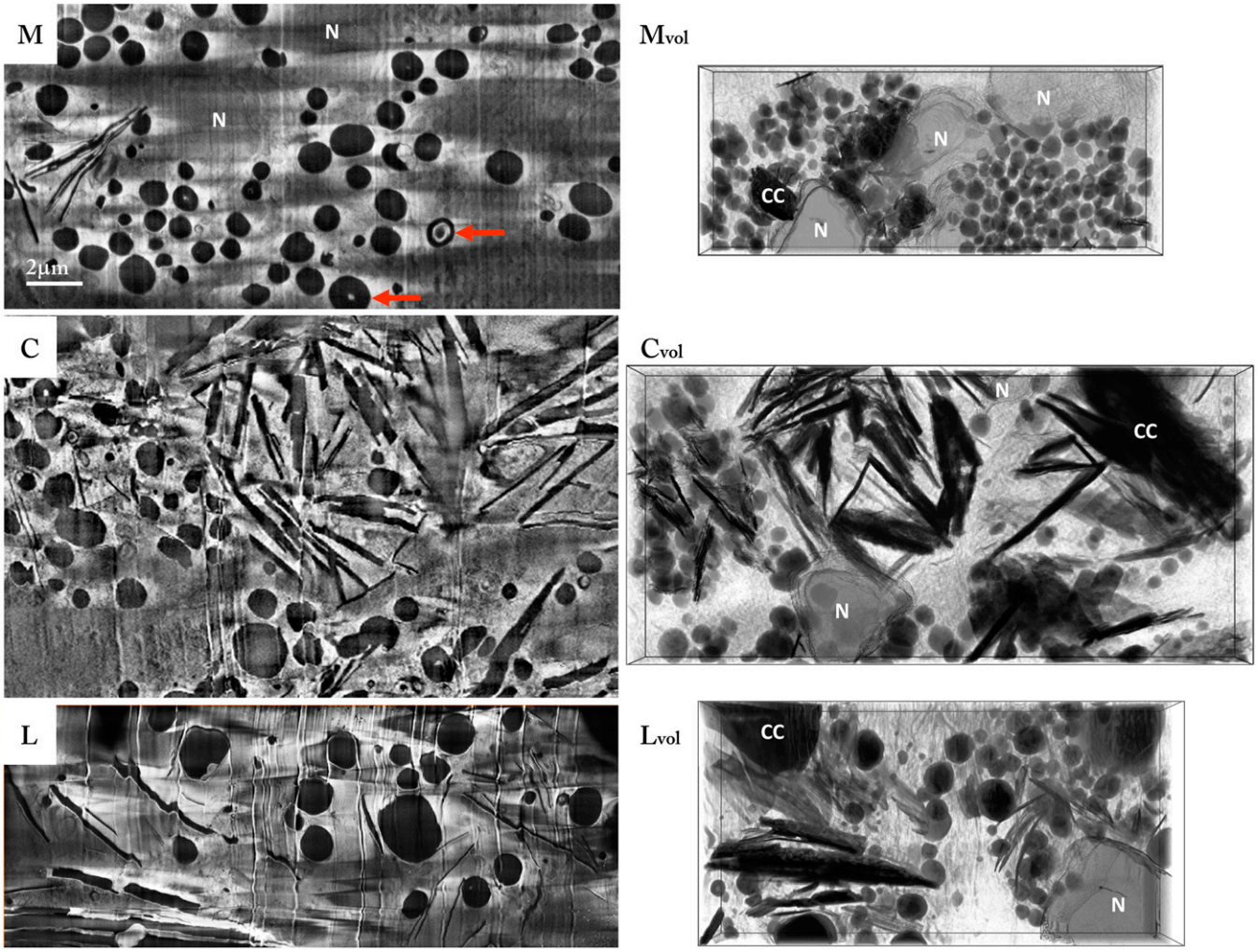

Fig. 2. Two-dimensional and 3D representation of the cryo-FIB-SEM stacks from M (region at the interface of the lesion with the tunica media of the blood vessel), C (core of lesion), and L (region of lesion bordering with the lumen). M, C, and L show representative slices of the three regions viewed in cryo-FIB-SEM. N, cell nucleus. Red arrows indicate heterogeneity in lipid droplet content. (Scale bar, 2 μm for M, C, and L.) M_{vol}, C_{vol}, and L_{vol} show segmented volume representations of the three regions presented to scale. N, cell nucleus; CC, cholesterol crystals. Dimensions of the displayed volumes are 25.6 × 10.3 × 3 μm^3 for M, 29.7 × 14.2 × 3 μm^3 for C, and 26.1 × 13.7 × 3 μm^3 for L. Compare to volume representations following automatic segmentation in *SI Appendix*, Fig. S5. For further details on image analysis see *Materials and Methods*.

larger lipid droplets (10% of the total volume), and detectable cell nuclei (Fig. 2, L and L_{vol}). We then focused on specific characteristics found in each examined region.

The M Region at the Interface of the Lesion with the Tunica Media. In the M region (Fig. 3 and Movie S1) there are mainly thin crystals, and judging from the proximity to intact nuclei and the partial cell membrane contours that we detect, the thin crystals are in intracellular locations (Fig. 3*A*). However, it is very difficult to determine, using imaging data alone, whether the crystals formed inside viable cells. For one cell in particular, it was possible to follow, in individual slices, the whole contour of the plasma membrane and the crystals inside it (Fig. 3*B*; compare with *SI Appendix*, Fig. S6 *A* and *B*), confirming that the crystals are in intracellular locations. The thin crystals are not enclosed within lysosomes, raising the possibility that they formed intracellularly.

The M volume is rich in lipid droplets that are intimately associated with thin crystals, such that it is difficult to distinguish between crystal and droplet surface in several locations (Fig. 3 *C* and *E*). Several thin crystals may be intimately associated with different surfaces of the same lipid droplet. We also consistently observed stacks of thin crystals, which still connect to the lipid droplet through the innermost crystal of the stack (Fig. 3*E*). We assume that each crystal formed on the surface of a lipid droplet and subsequently detached as a flat platelet from a curved droplet, making way for the next crystal nucleating on the same lipid droplet [Fig. 3 *E, (1)–(5)*]. Inside the lipid droplet, and in close proximity to nucleating crystals, we observed vacuolar structures, which are hypothesized to be hydrolysis pits (40), where cholesterol esters are hydrolyzed to cholesterol (Fig. 3 *E, (5)*, red arrowhead).

The C Region, the Plaque Core. The C region presents the highest amount of large plate-like cholesterol crystals that are independently positioned in the tissue, having no apparent association to lipid droplets or other cellular or extracellular structures (Fig. 4*A* and Movie S2). Similar to the M region, however, thin crystals appeared to be associated with lipid droplets in a region where lipid droplets appear (Fig. 4 *B* and *C*). We infer that thin crystal stacks could grow into stacks of thick crystals after losing contact with the lipid droplets. Thin crystals also appeared closely associated to the outermost membranous structures of multilamellar bodies (Fig. 4 *D* and *E*). Many lysosomal structures were observed, but none contained intralysosomal crystals.

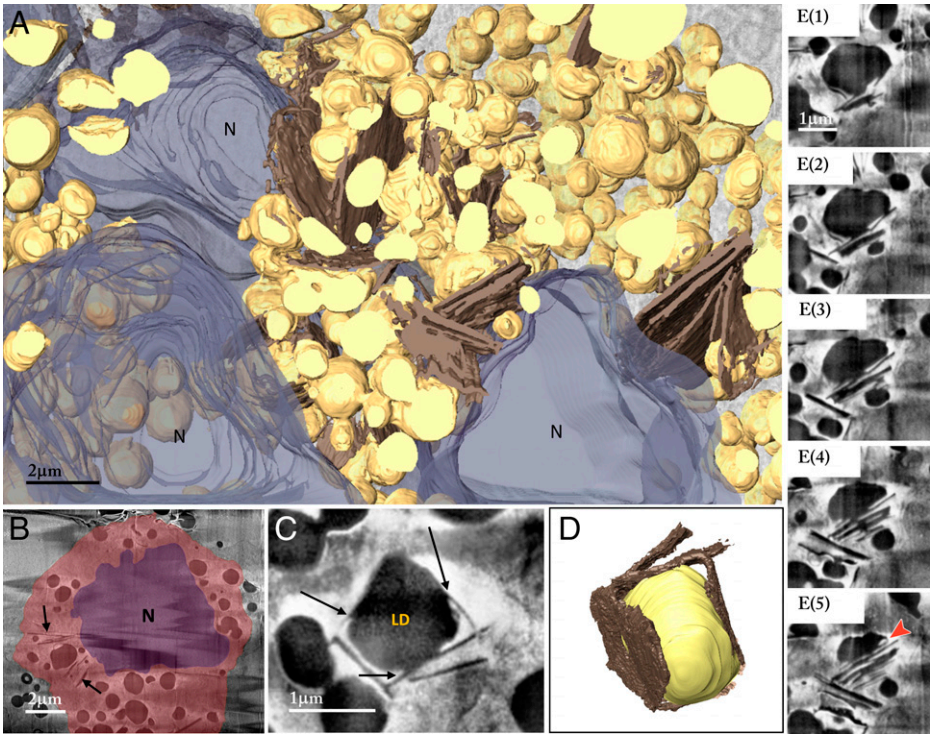

Fig. 3. Cryo-FIB-SEM images of the media-lesion interface region. (*A*) Surface representation of the segmented image stack. Lipid droplets yellow, cholesterol crystals brown, cell nuclei light purple. Volume thickness = 5 μm. (*B*) One slice, featuring a cell containing intracellular thin crystals (arrows) and lipid droplets. The plasma membrane can be followed along the whole perimeter of the cell (see raw image in *SI Appendix*, Fig. S6*A*). The cell area is pseudocolored in pink and the cell nucleus in purple. The nucleus of the cell shown in *B* is in the top left quadrant of the volume in *A*, but the left side of the cell containing the crystals is not included in the segmented frame. (*C*) Individual crystals attached to a lipid droplet. The crystals that are in closest contact with the lipid droplet surfaces merge with the lipid droplet (arrows). (*D*) Surface representation of the segmented lipid droplet/crystal complex shown in *C*. Color code in *D* is the same as in *A*. The apparent striation in the segmented thin crystals derives from the reconstruction/segmentation procedure. [*E(1)–(5)*] Progressive slices through the volume of the same object, separated by 100 to 150 nm, demonstrating stacking of thin crystals on a lipid droplet. Red arrowhead in *E5* indicates one of the vacuolar structures that is referred to as a hydrolysis pit (40).

The L Region Adjacent to the Vessel Lumen. In the L region, bordering with the vessel lumen, some lipid droplets were exceptionally large (up to 6 μm in diameter), a feature that was not observed in either of the other regions. Similar to the C region, large crystals were not related to any other cholesterol containing structures (Fig. 5*A* and Movie S3). Thin plate-like crystals with a high aspect ratio existed in this region as well, intimately associated with lipid droplets, and the thinnest crystals were observed inside the clearly membrane-delimited areas of two cells (Fig. 5 *B* and *C*; compare to *SI Appendix*, Fig. S6 *C–F*). As in Fig. 3*B*, the thin crystals are not enveloped by lysosomal membranes. Similar to the C region, multilamellar bodies are abundant and are occasionally associated with thin cholesterol crystals.

Cholesterol Crystal Morphology. Information on the crystal growth mechanisms can be derived also from observation of crystal morphologies (Fig. 6). Cholesterol crystals grown synthetically from water solution are rhomboidal thin plates with well-defined straight edges (Fig. 1 *I*, *Inset*). The thin dimension corresponds to a direction of slow growth relative to the other directions. As a rule of thumb, the younger the crystals are, the thinner they are, in agreement with what we would intuitively expect, namely, that thin newly formed crystals grow into thicker and larger crystals, maintaining their initial aspect ratio.

Some crystals from the M and from the L regions are so thin that they curve, wrapping around the lipid droplets from which they presumably get the cholesterol material for growth (Fig. 6*A*). The curved crystals may straighten up while thickening. From a random check of 20 crystals in each region of the cryo-FIB-SEM reconstructions that we segmented, the crystal thicknesses were within a range of 30 to 200 nm in region M, 100 to 1,000 nm in region C, and 30 to 850 nm in region L. Considering that the resolution is ∼20 to 30 nm, the thin crystals may well be even thinner than what we measured. The thinnest crystals were thus found in the M region and mostly were in confirmed intracellular locations.

The crystals in the lesions are for the most part not as regular as the synthetic crystals. The crystals in Fig. 6*B* have three straight edges, whereas the fourth edge is curved and irregular. This indicates that the crystals most probably grew in an aqueous medium, such as inside the cell or in the extracellular matrix, in contact with a curved surface, such as a cell membrane or a lipid droplet. The crystal in Fig. 6*C* is thin (<100 nm) but is adding additional layers to the crystal plate, as detectable from the stepped new edge on the plate face (indicated by black arrow). The warped irregular profile of the crystal shows that it grew in a crowded environment where physical barriers or additives that adsorbed on the edges retarded growth. The intertwined crystals in Fig. 6*D* grew together in a location where a high local concentration of cholesterol induced rapid nucleation and growth of several crystals in a limited space. Thus, information relevant to crystal formation and growth can be derived from the 3D dataset.

Discussion

We articulate the discussion along two lines, reflecting two different areas: the technical advancement in cryo-SEM, especially in three dimensions, and the consequences thereof within the area of atherosclerosis. The two subjects will be discussed separately.

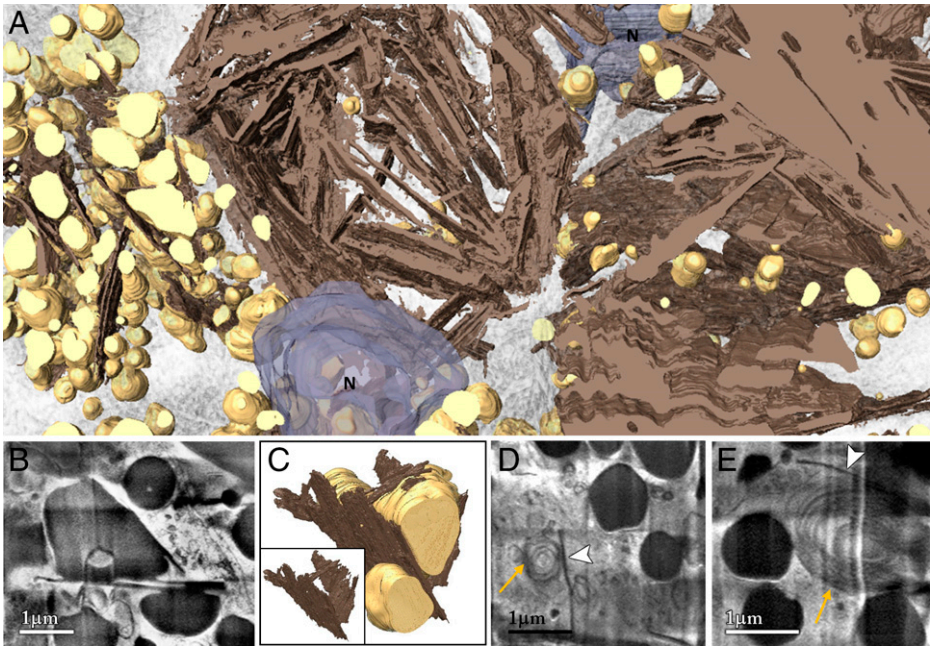

Fig. 4. Cryo-FIB-SEM images of the core region. (*A*) Surface representation of the segmented image stack. Color code as in Fig. 3. Volume dimensions = 30.92 × 13.58 × 5 μm^3. (*B*) One slice, featuring thin crystals attached and merged with two lipid droplets. (*C*) Surface representation of the segmented lipid droplet/crystal complex in *B*. (*Inset*) Crystal segmentation without the lipid droplets, emphasizing the different orientations of the crystal growth on the surface of the lipid droplet. The apparent striation in the segmented thin crystals derives from the reconstruction/segmentation procedure. (*D* and *E*) Lamellar bodies (yellow arrows) also appear attached to thin crystals (white arrowheads) but are less frequent than the lipid droplets.

High-Resolution Detection of Condensed Cholesterol Deposits in Tissues: The Technological Advancement. Cholesterol detection in an organic tissue by electron microscopy is not straightforward. Cholesterol crystals cannot be detected by backscattering because the cholesterol molecule contains carbon, oxygen, and hydrogen atoms only. Having no heavy atoms, it has no atomic number contrast and thus does not provide a measurable backscattering electrons signal. Furthermore, cholesterol crystals and lipid deposits dissolve during the preparation procedures used for conventional TEM, involving treatment with acetone and alcohol, which dissolve cholesterol and lipids (27, 41). After crystal dissolution, the TEM detects empty spaces reflecting the locations where the crystals were, rather than the crystals themselves (11, 16). Crystal dissolution in fact allows creation of contrast between the voids and the tissue, which would not exist between crystals and tissue, because both are composed of organic material with similar electron density.

In addition, conventional TEM sections undergo staining with heavy atoms that label specific components, such as cell membranes, which can artificially alter the inspected tissue. Finally, conventional TEM requires drying of the thin sections, which inevitably changes the void/tissue ratios. Specifically, drying of the samples makes it difficult, if not impossible, to evaluate localized interactions between crystals and lipid droplets, because both dissolve during sample preparation. As a consequence of all the above, cholesterol crystals were only documented in their native state by SEM in tissue samples that were dried but not treated with solvents, or after extraction from the tissue (1, 3). One recent study applied the technique of FIB-SEM block face sequential imaging to produce 3D images of relatively large

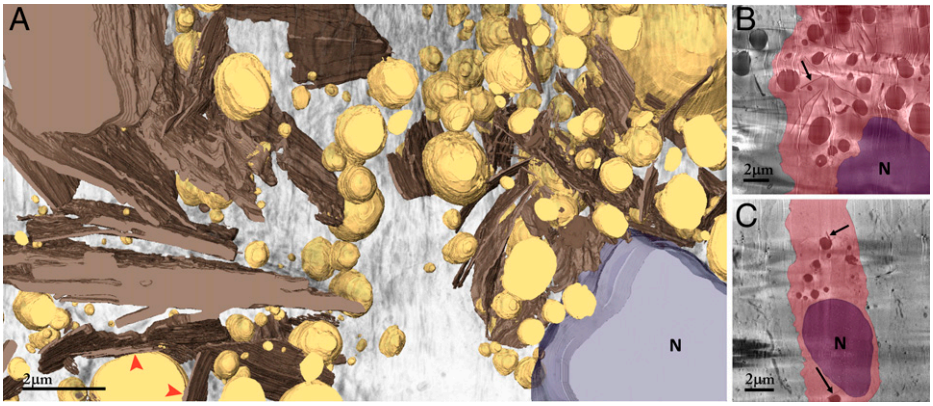

Fig. 5. Cryo-FIB-SEM images of the intimal region bordering with the lumen. (*A*) Surface representation of the segmented image stack. The large crystals on the left side of the image appear in the first slice of the imaged box in an oblique cut, which makes them appear thicker than they are. Two thin crystals are in contact with a lipid droplet (red arrowheads). Color code as in Fig. 3. Volume thickness 3 μm. The apparent striation in the segmented thin crystals derives from the reconstruction/segmentation procedure. (*B* and *C*) Two slices, featuring two cells containing intracellular thin crystals and lipid droplets. The plasma membrane can be followed along the perimeter of the cells that are visible in the slice (compare with raw images in *SI Appendix*, Fig. S6 *C* and *E*). Cell areas are pseudocolored in pink and the cell nuclei in purple. The thin crystals are inside the cells (black arrows).

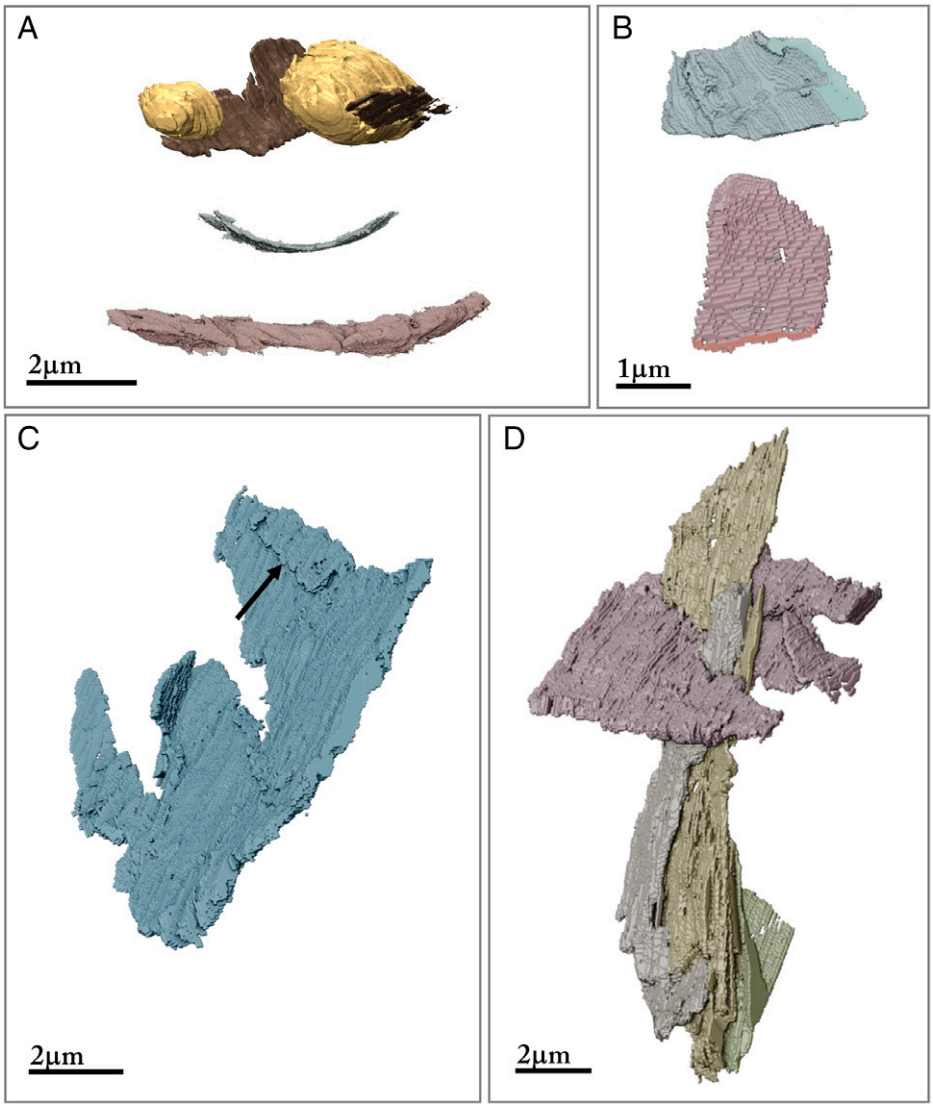

Fig. 6. Cryo-FIB-SEM segmented images of representative cholesterol crystals. (*A*) Crystals segmented from L, M and C regions. (*Top* and *Middle*) Thin curved crystals wrap around lipid droplets. (*Bottom*) Thicker crystals gradually straighten up. (*B–D*) Crystals segmented from the core region. (*B*) Single crystals having regions delimited by well-defined crystal faces. (*C*) Thin crystal displaying growth steps (black arrow). (*D*) Conglomerate of intergrown crystals. For further image analysis details see *Materials and Methods*.

volumes (tens of micrometers wide) from a human atheroma. The 3D reconstructions and segmentations are impressive and informative, although the study involved embedding in resin, drying, and staining of the tissue and thus suffered from the limitations mentioned above (22).

Here we used only cryo-techniques, which have both the advantages of preserving the cholesterol deposits and of preserving the tissues hydrated. The absence of contrast between crystals and tissue was resolved in two different ways: Cholesterol and cholesteryl esters give rise to strong CL signals, and thus are visible in the freeze-fractured surface using the CL detector at the SEM (35–38, 42, 43). We thus developed a correlative workflow that uses CL and cryo-SEM to detect the lesion regions characterized by large cholesterol deposits, which could be further examined in 3D at high magnification. We also note that CL light emission identifies the presence of cholesterol and cholesterol esters, avoiding confusion between cholesterol deposits and calcifications, which [according to Sarig et al. (36)] have a very faint CL signal, or no signal at all, while displaying strong backscattering signal.

We obtained two-dimensional (2D) topographic images at nanometer-scale resolution, as well as 3D volume reconstructions and segmentations at 20-nm resolution, of intact cholesterol crystals and lipid deposits within hydrated tissues.

The insights that we derived using this combination of cryo-techniques are discussed below.

Examination of Atherosclerotic Tissues. Using cryo-SEM we could distinguish between regions in the lesion displaying some degree of order, with recognizable tissue architecture, and completely disordered regions including large deposits of crystalline cholesterol. The partially ordered regions were characterized by a substantial intra- and extracellular population of lipid droplets and a limited amount of crystalline cholesterol, consisting of thin crystals intimately associated with lipid droplets.

Using cryo-FIB-SEM, we observed three regions situated at the lesion border with the media (M), in the core of the lesion (C), and in the intimal region bordering with the vessel lumen (L), respectively. Judging from the presence of intact cells and close to normal tissue architecture, the M region is the region least affected by the lesion. Lipid droplets and stacks of very thin crystalline cholesterol plates appear mostly enclosed within foam cells, but also in extracellular locations.

As expected (26), in the core there is a large amount of cholesterol crystals, including both large and thick (200 to 1,000 nm thick) plate-like crystals and smaller and thin (few tens of nanometers to 200 nm thick) platy crystals that are intimately associated with the surfaces of lipid droplets, similar to those observed in the M region. As far as we could see, there are fewer cells in the C region, but the thinnest crystals in this region appear in the same locations as the detectable cell nuclei and lipid droplets.

Lipid droplets originate in the endoplasmic reticulum of living cells, where they function as lipid and cholesterol storage (11). We see here strong evidence that lipid droplets can induce nucleation and growth of cholesterol crystals. In support of this statement, we note that the thinnest crystals ($\leq$30 nm thick) are intimately associated with lipid droplets, often to the point that they appear fused to the droplet and wrap around it. The crystal thickness indicates that the crystal is in the first stages of formation, close to nucleation. As neutral hydrolase in lipid droplets hydrolyzes cholesteryl ester to generate free cholesterol (11), it is not surprising that lipid droplet surfaces can provide active sites for cholesterol crystal nucleation (44). The opposite process, where cholesterol crystals might be actively solubilized by esterification on the lipid droplet surface, is not likely, due to the progressive overload of intracellular cholesterol in the cells caused by a continuous cholesterol supply (10, 11). Additionally, pits in the peripheral regions of lipid droplets, similar to those that we observed close to the forming crystals [Fig. 3 *E*, *(5)*], were attributed to "pockets" where cholesteryl ester hydrolysis occurs (40).

There is a widespread belief that cholesterol crystals in atherosclerotic lesions can appear inside cells only if they have been phagocytosed from the external medium where they formed (22). While we do not exclude that crystals form extracellularly, we observed in the M region and in the L region nascent crystals associated to lipid droplets, inside cells enclosed by a continuous plasma membrane. We suggest that these crystals formed inside the cells because they are extremely thin and, besides, phagocytosed crystals would appear enclosed in lysosomal compartments. It is worth noting a study showing that foam cells did not completely lose their ability to process excess cholesterol, even after accumulating large amounts of lipids and after considerable time within the lesions (45).

The presence, in all regions, of two different crystalline subpopulations, mature large isolated crystals and thin crystals intimately associated with lipid droplets, can imply either of two scenarios. The two crystal types can be part of a continuous process that starts with nucleation on lipid droplet surfaces and is followed by progressive growth, until the large crystals form. The alternative is that two independent routes exist for crystal formation: The first is nucleation from intracellular or extracellular lipid droplets, whereas in the second route cholesterol crystals nucleate and grow from cholesterol coming from extracellular sources (22). In either case, the ubiquitous presence of crystals in very early stages of growth indicates that fresh crystals form at all times in all the regions of the plaque, including the core.

Interestingly, the recent study involving FIB-SEM within human atherosclerotic lesions showed association between a large (>1 μm thick) elongated cholesterol crystal and a lipid droplet and raised the possibility that cholesterol crystals may grow out from large lipid droplets (22). This may indeed be the case, but the mature stage of crystal development makes it difficult to relate the observation to the nucleation event. Rod-like crystals were extracted in the past from atherosclerotic lesions, together with plate-like crystals (46). We previously observed that elongated crystals form from macrophages cultured with LDL, and the elongated morphology indicated their original formation in the monoclinic, metastable polymorph of cholesterol monohydrate crystals (19, 47–49). We did not observe, however, similar elongated crystals in the present study.

Lamellar bodies, consisting of cholesterol and phospholipids, are associated with the extracellular matrix of the intima in early and late regions of atherosclerotic plaques (50). Thin cholesterol crystals also appeared associated with the external membranes of lamellar bodies, especially in the core region, but not within their inner compartments. Excess cholesterol is solubilized also with the help of the phospholipid layers of multilamellar bodies, which could also serve as reservoir of cholesterol and nucleation sites for further crystallization (15, 17). In support of this option, we observed in the cultured macrophage model systems, crystal formation in locations associated with the plasma membrane and other cell membranes (19, 51). TEM studies, performed on rabbits fed with high-cholesterol diet for up to 5 mo, indicated that lysosomes might serve as storage sites of free and esterified cholesterol. Some lysosomal lipid inclusions are crystalline, suggesting that they might originate from cholesterol or cholesteryl esters (15, 52). However, the possibility that crystalline inclusions in lysosomes and intracellular inclusions in general may have formed in the extracellular matrix could not be excluded.

The L region is also rich in large cholesterol crystals, similar to those of the C region, and in smaller thin platy crystals associated with lipid droplets as in regions M and C. Additionally, lipid bodies were found to be heterogeneous in size, in part considerably larger (up to 6 μm in diameter) than in the M or C regions. These combined observations might suggest different cholesterol processing in this region. LDL delivery occurs from the intimal site (53). Part of the lipid bodies and crystals may be relatively mature and may result from translocation of cholesterol deposits from the endothelial region (54, 55). In possible agreement with this interpretation is the notion that in advanced lesions most of the foam cells are found closer to the core regions (45), while the region proximal to the lumen is mostly occupied by endothelial cells, which process cholesterol differently (55). Although endothelial cells are in constant contact with LDL, their LDL processing and its effect on atherogenesis remain ambiguous. It is generally assumed that LDL taken up by endothelial cells is transcytosed through the cell and deposited into the intima (55, 56). Rambold et al. established that lipid droplets in starved fibroblasts can be secreted to extracellular locations due to the limited lipid droplet storage capacity in cells of nonadipose origin (55, 57). In any case, it is likely that several different processes occur in parallel in the L region.

Concluding Remarks

In rabbit animal models of atherosclerosis, the cholesterol metabolism and spontaneous lesion development are similar to the human, but lesion formation occurs in a limited time (weeks), as opposed to decades of maturation in the atherosclerotic lesion of human patients. This is a great advantage, because the disease develops under controlled conditions and can be followed in time. On the other hand, for the same reasons, direct transfer of any hypotheses derived from studies on rabbits to human lesions must be considered carefully.

With all due caution, our observations lead us to bring forward two concepts: 1) Cholesterol crystal nucleation occurs on lipid droplets or on multilamellar bodies and 2) cholesterol crystals do nucleate also inside cells. The two observations are

part of the same conceptual framework, because lipid droplets and multilamellar bodies originate inside viable cells. The mechanism that emerges for crystal formation is, however, not exclusive; rather, it leaves ample space for additional processes of crystal nucleation and growth to occur in parallel.

The above findings became possible by virtue of the complex technical combination of cryo-CL with cryo-SEM and cryo-FIB-SEM. This combination can be useful in other systems where cholesterol deposits occur in tissues.

Materials and Methods

Rabbit atherosclerotic lesions were initiated and dissected following an established protocol (58). Further details are given in *SI Appendix, Materials and Methods*.

All animal experiments were performed with the approval of the Animal Care Committee of the University of Yamanashi and conformed to the *Guide for the Care and Use of Laboratory Animals* published by the National Institutes of Health (59).

After undergoing transverse slicing to a thickness of 100 to 200 μm and 0.5- to 1-mm width, the samples were high-pressure-frozen and freeze-fractured as described (28) prior to observation in the cryo-SEM or cryo-FIB-SEM (*SI Appendix, Materials and Methods*).

Imaging Techniques. The protocols for all imaging techniques are individually described in *SI Appendix, Materials and Methods*.

Histology was performed following standard procedures.

Cryo-SEM. Tissues were examined in hydrated vitrified conditions as described (28, 29).

CL. Cholesterol CL was documented in the early 1990s (35–38). The sample is excited with an electron beam in the electron microscope under cryogenic conditions, and the emitted light is collected and imaged using a photomultiplier tube in panchromatic mode.

Cryo-FIB-SEM. High-pressure-frozen and freeze-fractured samples were first observed in the scanning electron microscope in SE and CL modes to identify the regions of interest. The samples were then transferred to the FIB-SEM preserving at all times cryogenic conditions, and trenches were carved in the identified locations. Acquisition of serial images was performed as described in ref. 32 and is reported in detail in *SI Appendix, Materials and Methods*.

Image Analysis. The images were aligned and artifacts were partially removed as described (29, 32, 60). Data were then segmented automatically (*SI Appendix*, Fig. S5) and manually (Figs. 2–6) in volume and surface representations (*SI Appendix, Materials and Methods*).

Data Availability. All study data are included in the article and/or supporting information.

ACKNOWLEDGMENTS. We thank Dr. Eyal Shimoni for helping us with the effort associated with cryo-SEM. We thank Dr. Luca Bertinetti for providing the algorithm needed for cryo-FIB-SEM data analysis. All of the electron microscopy studies were conducted at the Irving and Cherna Moskowitz Center for Nano and Bio-Nano Imaging at the Weizmann Institute of Science. This research is made possible in part by the historic generosity of the Harold Perlman Family. Financial support was provided by the Binational Science Foundation grant (application number 2019087).

Author affiliations: [a]Department of Chemical and Structural Biology, Weizmann Institute of Science, 7610001 Rehovot, Israel; [b]Department of Chemical Research Support, Weizmann Institute of Science, 7610001 Rehovot, Israel; [c]Experimental Atherosclerosis Section, NIH, Bethesda, MD 20892; and [d]Department of Molecular Pathology, University of Yamanashi, Yamanashi 409-3898, Japan

1. G. S. Abela, Cholesterol crystals piercing the arterial plaque and intima trigger local and systemic inflammation. *J. Clin. Lipidol.* **4**, 156–164 (2010).
2. J. Dai *et al.*, Association between cholesterol crystals and culprit lesion vulnerability in patients with acute coronary syndrome: An optical coherence tomography study. *Atherosclerosis* **247**, 111–117 (2016).
3. G. S. Abela, K. Aziz, Cholesterol crystals cause mechanical damage to biological membranes: A proposed mechanism of plaque rupture and erosion leading to arterial thrombosis. *Clin. Cardiol.* **28**, 413–420 (2005).
4. P. Duewell *et al.*, NLRP3 inflammasomes are required for atherogenesis and activated by cholesterol crystals. *Nature* **464**, 1357–1361 (2010).
5. A. Grebe, E. Latz, Cholesterol crystals and inflammation. *Curr. Rheumatol. Rep.* **15**, 313 (2013).
6. D. M. Small, George Lyman Duff memorial lecture. Progression and regression of atherosclerotic lesions. Insights from lipid physical biochemistry. *Arteriosclerosis* **8**, 103–129 (1988).
7. X. Li, G. Bayliss, S. Zhuang, Cholesterol crystal embolism and chronic kidney disease. *Int. J. Mol. Sci.* **18**, 1120 (2017).
8. C. Shi *et al.*, Crystal clots as therapeutic target in cholesterol crystal embolism. *Circ. Res.* **126**, e37–e52 (2020).
9. Y. Baumer, N. N. Mehta, A. K. Dey, T. M. Powell-Wiley, W. A. Boisvert, *Cholesterol Crystals and Atherosclerosis* (Oxford University Press, 2020).
10. H. S. Kruth, Macrophage foam cells and atherosclerosis. *Front. Biosci.* **6**, D429–D455 (2001).
11. D. A. Chistiakov, Y. V. Bobryshev, A. N. Orekhov, Macrophage-mediated cholesterol handling in atherosclerosis. *J. Cell. Mol. Med.* **20**, 17–28 (2016).
12. M. Ouimet, T. J. Barrett, E. A. Fisher, HDL and reverse cholesterol transport. *Circ. Res.* **124**, 1505–1518 (2019).
13. A. Janoudi, F. E. Shamoun, J. K. Kalavakunta, G. S. Abela, Cholesterol crystal induced arterial inflammation and destabilization of atherosclerotic plaque. *Eur. Heart J.* **37**, 1959–1967 (2016).
14. S. S. Katz, G. G. Shipley, D. M. Small, Physical chemistry of the lipids of human atherosclerotic lesions. Demonstration of a lesion intermediate between fatty streaks and advanced plaques. *J. Clin. Invest.* **58**, 200–211 (1976).
15. F. Lupu, I. Danaricu, N. Simionescu, Development of intracellular lipid deposits in the lipid-laden cells of atherosclerotic lesions. A cytochemical and ultrastructural study. *Atherosclerosis* **67**, 127–142 (1987).
16. R. K. Tangirala *et al.*, Formation of cholesterol monohydrate crystals in macrophage-derived foam cells. *J. Lipid Res.* **35**, 93–104 (1994).
17. A. M. Klinkner, C. R. Waites, W. D. Kerns, P. J. Bugelski, Evidence of foam cell and cholesterol crystal formation in macrophages incubated with oxidized LDL by fluorescence and electron microscopy. *J. Histochem. Cytochem.* **43**, 1071–1078 (1995).
18. G. Kellner-Weibel *et al.*, Crystallization of free cholesterol in model macrophage foam cells. *Arterioscler. Thromb. Vasc. Biol.* **19**, 1891–1898 (1999).
19. N. Varsano *et al.*, Two polymorphic cholesterol monohydrate crystal structures form in macrophage culture models of atherosclerosis. *Proc. Natl. Acad. Sci. U.S.A.* **115**, 7662–7669 (2018).
20. G. N. Ioannou *et al.*, Cholesterol crystallization within hepatocyte lipid droplets and its role in murine NASH [S]. *J. Lipid Res.* **58**, 1067–1079 (2017).
21. G. N. Ioannou *et al.*, Cholesterol crystals in hepatocyte lipid droplets are strongly associated with human nonalcoholic steatohepatitis. *Hepatol. Commun.* **3**, 776–791 (2019).
22. S. Lehti *et al.*, Extracellular lipids accumulate in human carotid arteries as distinct three-dimensional structures and have proinflammatory properties. *Am. J. Pathol.* **188**, 525–538 (2018).
23. T. M. Bocan, T. A. Schifani, J. R. Guyton, Ultrastructure of the human aortic fibrolipid lesion. Formation of the atherosclerotic lipid-rich core. *Am. J. Pathol.* 123, 413–424 (1986).
24. J. Fan *et al.*, Rabbit models for the study of human atherosclerosis: From pathophysiological mechanisms to translational medicine. *Pharmacol. Ther.* **146**, 104–119 (2015).
25. W. C. Dornas, T. T. Oliveira, L. E. F. Augusto, T. J. Nagem, Experimental atherosclerosis in rabbits. *Arq. Bras. Cardiol.* **95**, 272–278 (2010).
26. C. W. Adams, O. B. Bayliss, Crystals in atherosclerotic lesions: Real or artefact? *Atherosclerosis* **22**, 629–636 (1975).
27. M. Nasiri *et al.*, Role of cholesterol crystals in atherosclerosis is unmasked by altering tissue preparation methods. *Microsc. Res. Tech.* **78**, 969–974 (2015).
28. N. Varsano *et al.*, Development of correlative cryo-soft X-ray tomography and stochastic reconstruction microscopy. A study of cholesterol crystal early formation in cells. *J. Am. Chem. Soc.* **138**, 14931–14940 (2016).
29. N. Varsano *et al.*, Characterization of the growth plate-bone interphase region using cryo-FIB SEM 3D volume imaging. *J. Struct. Biol.* **213**, 107781 (2021).
30. A. Schertel *et al.*, Cryo FIB-SEM: Volume imaging of cellular ultrastructure in native frozen specimens. *J. Struct. Biol.* **184**, 355–360 (2013).
31. N. Vidavsky *et al.*, Cryo-FIB-SEM serial milling and block face imaging: Large volume structural analysis of biological tissues preserved close to their native state. *J. Struct. Biol.* **196**, 487–495 (2016).
32. D. Spehner *et al.*, Cryo-FIB-SEM as a promising tool for localizing proteins in 3D. *J. Struct. Biol.* **211**, 107528 (2020).
33. M. P. Jokinen, T. B. Clarkson, R. W. Prichard, Animal models in atherosclerosis research. *Exp. Mol. Pathol.* **42**, 1–28 (1985).
34. E. A. Schenk, E. Gaman, A. Feigenbaum, Spontaneous aortic lesions in rabbits I. Morphologic characteristics. *Circ. Res.* **19**, 80–88 (1966).
35. T. Nakano, T. Fujimoto, H. Koike, K. Ogawa, Application of analytical color fluorescence electron microscopy to biomedical field: II. Cholesterol ester in rat adrenal cortex. *Acta Histochem. Cytochem.* **23**, 769–780 (1990).
36. S. Sarig *et al.*, Apatite-cholesterol agglomerates in human atherosclerotic lesions. *Cells Mater.* **2**, 7 (1992).
37. G. Ning, T. Fujimoto, H. Koike, K. Ogawa, Cathodoluminescence-emitting lipid droplets in rat testis: A study by analytical color fluorescence electron microscopy. *Cell Tissue Res.* **271**, 217–225 (1993).
38. A. S. Loginov *et al.*, Investigation of cholesterol, bilirubin, and protein distribution in human gallstones by color cathodoluminescence scanning electron microscopy and transmission electron microscopy. *Scanning* **20**, 17–22 (1998).
39. J. Mahamid *et al.*, Liquid-crystalline phase transitions in lipid droplets are related to cellular states and specific organelle association. *Proc. Natl. Acad. Sci. U.S.A.* **116**, 16866–16871 (2019).
40. J. R. Guyton, K. F. Klemp, The lipid-rich core region of human atherosclerotic fibrous plaques. Prevalence of small lipid droplets and vesicles by electron microscopy. *Am. J. Pathol.* **134**, 705–717 (1989).
41. L. Graham, J. M. Orenstein, Processing tissue and cells for transmission electron microscopy in diagnostic pathology and research. *Nat. Protoc.* **2**, 2439–2450 (2007).

42. K. Keevend *et al.*, Tb^{3+}-doped LaF_3 nanocrystals for correlative cathodoluminescence electron microscopy imaging with nanometric resolution in focused ion beam-sectioned biological samples. *Nanoscale* **9**, 4383–4387 (2017).
43. K. Keevend, T. Coenen, I. K. Herrmann, Correlative cathodoluminescence electron microscopy bioimaging: Towards single protein labelling with ultrastructural context. *Nanoscale* **12**, 15588–15603 (2020).
44. M. Shepelenko *et al.*, Polymorphism, structure, and nucleation of cholesterol·H_2O at aqueous interfaces and in pathological media: Revisited from a computational perspective. *J. Am. Chem. Soc.* **144**, 5304–5314 (2022).
45. M. E. Rosenfeld, R. Ross, Macrophage and smooth muscle cell proliferation in atherosclerotic lesions of WHHL and comparably hypercholesterolemic fat-fed rabbits. *Arteriosclerosis* **10**, 680–687 (1990).
46. H. S. Kruth, Cholesterol deposition in atherosclerotic lesions. *Subcell. Biochem.* **28**, 319–362 (1997).
47. I. Solomonov, M. J. Weygand, K. Kjaer, H. Rapaport, L. Leiserowitz, Trapping crystal nucleation of cholesterol monohydrate: Relevance to pathological crystallization. *Biophys. J.* **88**, 1809–1817 (2005).
48. R. Ziblat, L. Leiserowitz, L. Addadi, Crystalline domain structure and cholesterol crystal nucleation in single hydrated DPPC:cholesterol:POPC bilayers. *J. Am. Chem. Soc.* **132**, 9920–9927 (2010).
49. N. Varsano, I. Fargion, S. G. Wolf, L. Leiserowitz, L. Addadi, Formation of 3D cholesterol crystals from 2D nucleation sites in lipid bilayer membranes: Implications for atherosclerosis. *J. Am. Chem. Soc.* **137**, 1601–1607 (2015).
50. G. Schmitz, G. Müller, Structure and function of lamellar bodies, lipid-protein complexes involved in storage and secretion of cellular lipids. *J. Lipid Res.* **32**, 1539–1570 (1991).
51. D. S. Ong *et al.*, Extracellular cholesterol-rich microdomains generated by human macrophages and their potential function in reverse cholesterol transport. *J. Lipid Res.* **51**, 2303–2313 (2010).
52. H. Shio, N. J. Haley, S. Fowler, Characterization of lipid-laden aortic cells from cholesterol-fed rabbits. III. Intracellular localization of cholesterol and cholesteryl ester. *Lab. Invest.* **41**, 160–167 (1979).
53. E. Vasile, M. Simionescu, N. Simionescu, Visualization of the binding, endocytosis, and transcytosis of low-density lipoprotein in the arterial endothelium in situ. *J. Cell Biol.* **96**, 1677–1689 (1983).
54. I. Gonçalves *et al.*, Short communication: Dating components of human atherosclerotic plaques. *Circ. Res.* **106**, 1174–1177 (2010).
55. Y. Baumer *et al.*, Hyperlipidemia-induced cholesterol crystal production by endothelial cells promotes atherogenesis. *Nat. Commun.* **8**, 1129 (2017).
56. H. S. Kruth, Subendothelial accumulation of unesterified cholesterol. An early event in atherosclerotic lesion development. *Atherosclerosis* **57**, 337–341 (1985).
57. A. S. Rambold, S. Cohen, J. Lippincott-Schwartz, Fatty acid trafficking in starved cells: Regulation by lipid droplet lipolysis, autophagy, and mitochondrial fusion dynamics. *Dev. Cell* **32**, 678–692 (2015).
58. M. Niimi *et al.*, Probucol inhibits the initiation of atherosclerosis in cholesterol-fed rabbits. *Lipids Health Dis.* **12**, 166 (2013).
59. National Research Council, Guide to the Care and Use of Laboratory Animals (National Academies Press, Washington, DC, 8th ed., 2011).
60. L. Vincent, Morphological grayscale reconstruction in image analysis: Applications and efficient algorithms. *IEEE Trans. Image Process.* **2**, 176–201 (1993).